analytical chemistry

Article

Cite This: Anal. Chem. 2018, 90, 3227−3237

pubs.acs.org/ac

Improved Quantitative SERS Enabled by Surface Plasmon Enhanced Elastic Light Scattering

Haoran Wei,[†,‡,§] Weinan Leng,[†,‡,§] Junyeob Song,[∥] Marjorie R. Willner,[†,‡,§] Linsey C. Marr,[†,‡,§] Wei Zhou,[∥] and Peter J. Vikesland*[,†,‡,§]

[†]Department of Civil and Environmental Engineering, Virginia Tech, Blacksburg, Virginia 24061, United States

[‡]Virginia Tech Institute of Critical Technology and Applied Science (ICTAS) Sustainable Nanotechnology Center (VTSuN), Blacksburg, Virginia 24061, United States

[§]Center for the Environmental Implications of Nanotechnology (CEINT), Duke University, Durham, North Carolina 27708, United States

[∥]Department of Electrical and Computer Engineering, Virginia Tech, Blacksburg, Virginia 24060, United States

Supporting Information

ABSTRACT: The application of surface-enhanced Raman spectroscopy (SERS) for everyday quantitative analysis is hindered by the point-to-point variability of SERS substrates that arises due to the heterogeneous distribution of localized electromagnetic fields across a suite of plasmonic nanostructures. Herein, we adopt surface-enhanced elastic scattering as a SERS internal standard. Both elastic and inelastic (i.e., Raman) scattering are simultaneously enhanced by a given "hot spot", and thus, the surface-enhanced elastic scattering signal provides a localized intrinsic internal standard that scales across all of the plasmon-enhanced electromagnetic fields within a substrate. Elastically scattered light originates from the amplified spontaneous emission (ASE) of the commercial laser, leading to the formation of a low-wavenumber pseudo band that arises from the interaction of the ASE and the edge filter. A theoretical model was developed to illustrate the underlying mechanism supporting this normalization approach. The normalized Raman signals are independent of the incident laser intensity and the density of "hot spots" for numerous SERS substrates. Following "hot-spot" (HS) normalization, the coefficient of variation for the tested SERS substrates decreases from 10 to 60% to 2%−7%. This approach significantly improves SERS quantitation of four chloroanilines and enables collection of highly reproducible analyte adsorption results under both static and dynamic imaging conditions. Overall, this approach provides a simple means to improve SERS reproducibility without the need to use additional chemicals as internal standards.

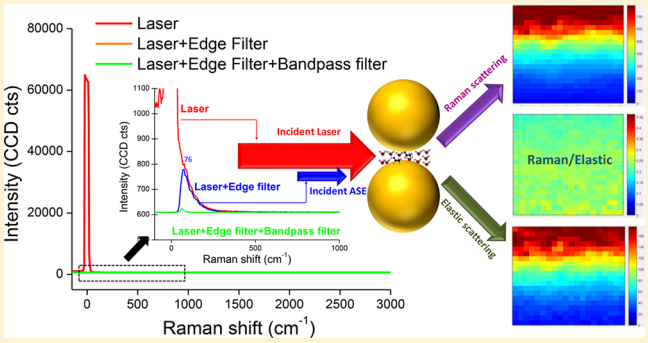

Surface-enhanced Raman spectroscopy (SERS) has long been proposed as an ultrasensitive analysis method with single molecule sensitivity, minimal need for sample pretreatment, rapid detection time, and potential for on-site deployment.[1−5] However, in spite of the volume of research conducted to develop SERS substrates and optimize the technique, the poor reproducibility of the SERS signal makes it a challenge to achieve reliable quantitative analysis. SERS largely remains a laboratory curiosity, but with great potential for multiple real-world applications.[6−9] One means to improve SERS reproducibility is to develop uniform SERS substrates through "top-down" nanofabrication.[10−15] However, it is challenging to create such substrates at scale and at reasonable cost.

An alternative approach to improve SERS reproducibility is to incorporate internal standards (IS) into the substrate.[16−19] The IS undergoes the same enhancement as target analytes, thus reducing point-to-point variability in the signal caused by substrate heterogeneity, laser intensity fluctuations, or temperature variation. Although SERS quantitation can be achieved using an IS, it adds to the cost and complexity of substrate preparation, lacks universal applicability, generates interferent Raman bands, and the reference probe molecules may occupy SERS "hot spots". In addition, it is nontrivial to find an appropriate IS that reflects the chemical and physical properties of the target analyte. Isotope-edited internal standards (IEIS) are ideal candidates for IS because the isotope analogues have the same Raman cross-section and the same affinity to the plasmonic surface.[19,20] While analyte concentrations can be determined based on the ratios of the Raman band intensities of the two isotope analogues, their adsorption kinetics cannot be acquired. In addition, IEIS for a large number of chemicals

Received: November 12, 2017
Accepted: January 22, 2018
Published: January 22, 2018

DOI: 10.1021/acs.analchem.7b04667
Anal. Chem. 2018, 90, 3227−3237

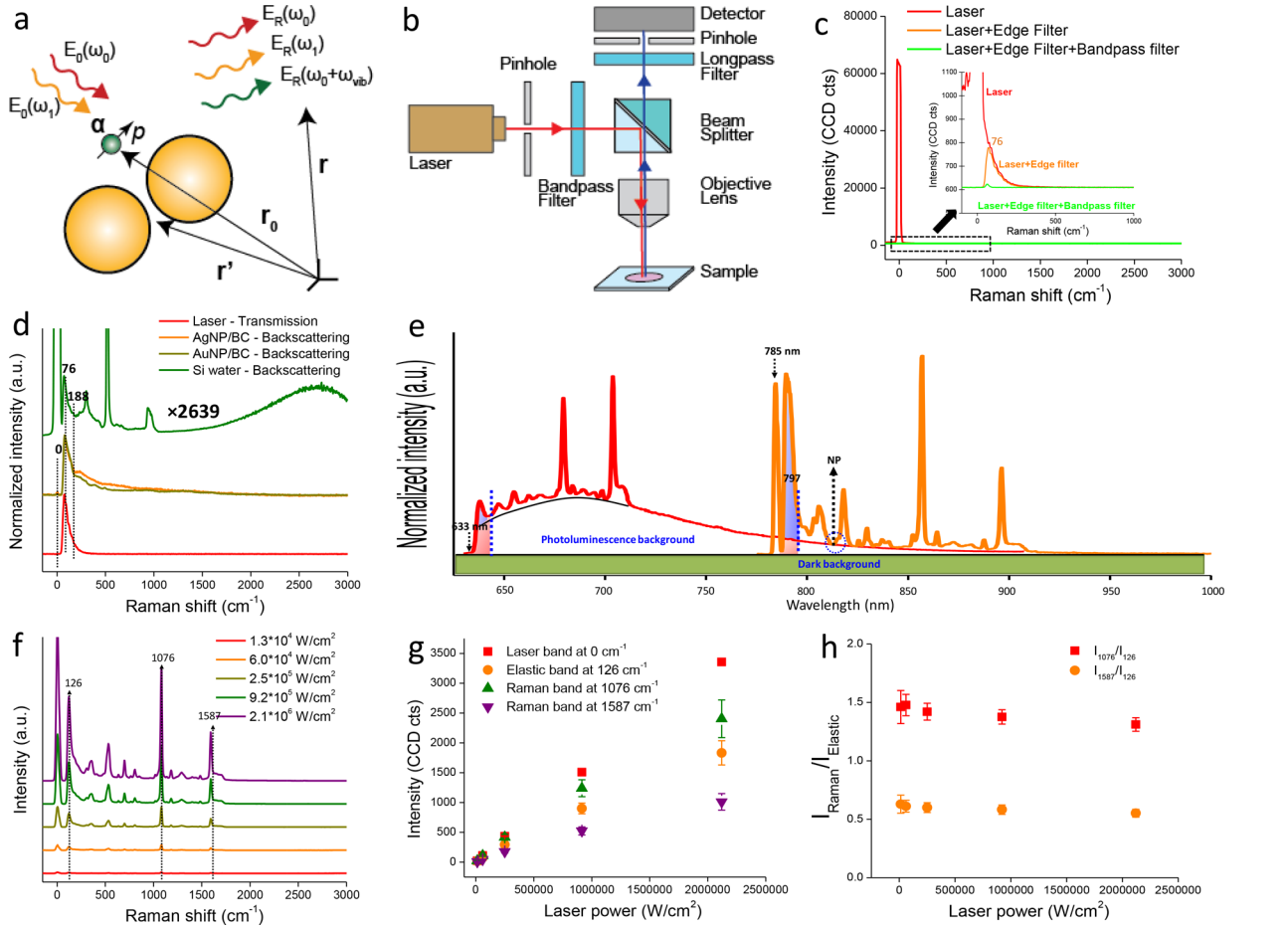

Figure 1. (a) Schematic illustration of the relation between the incident field (E_0) and scattered (E_R) elastic and Raman fields passing through a "hot spot". (b) The system employed for backscattering confocal Raman microspectroscopy/imaging. (c) Laser emission spectra in transmission mode with or without an edge or bandpass filter. (d) Raman spectra of two SERS substrates and Si wafer collected using backscattering Raman mode compared to transmission mode laser emission spectra. (e) Raman spectra of AuNP/BC exposed to 4-MBA excited by 633 and 785 nm lasers. The spectra are normalized to the intensity at 813 nm (= normalization point (NP)). Blue and red shaded areas represent contribution of elastic scattering and photoluminescence (PL), respectively, to ν_e. (f) Raman spectra of 4-mercaptobenzoic acid (4-MBA) under various laser powers (band assignments in Table S1). (g) Variation of band intensities of the laser peak, ν_e at 126 cm^{-1}, and the principal 4-MBA bands at 1076 and 1587 cm^{-1} as a function of laser power. (h) Variation of the intensity ratio between the 4-MBA bands at 1076 and 1587 cm^{-1} and the ν_e pseudopeak (at 126 cm^{-1}) as a function of laser power.

of analytical interest are not readily available. Importantly, none of the aforementioned approaches is applicable for SERS sensing under dynamic conditions wherein "hot spot" densities change over time. Such conditions are prevalent in SERS assays for biomedical and environmental detection.[21−25]

The SERS effect is inherently surface enabled with the highest signal enhancements observed at locations where the electromagnetic field is highest (i.e., either at edges or between two nanoparticles).[9,26] Regions with the highest enhancement factors are typically referred to as SERS "hot spots". Variation of SERS signals induced by the heterogeneous distribution of "hot spots" oftentimes surpasses that induced by the change of analyte concentrations on NP surfaces. Therefore, normalizing "hot spot" distribution across a single substrate or among different substrates is vitally important for improving the performance of SERS quantitation. It was recently reported that the elastic scattering undergoes the same electromagnetic enhancement as the inelastic scattering coming from the same SERS "hot spot".[27] Based on this study and considering the intrinsic drawbacks of the reported IS, we sought to explore the relationship between the measured elastic scattering signal and the SERS signal intensity.

In this effort, we demonstrate a simple approach for improving SERS reproducibility that exploits surface plasmon enhanced elastic scattering signals as internal standards for SERS signal normalization. Both theory and experiments show that the intensity of the surface plasmon enhanced elastic scattering signal of a low-wavenumber pseudoband (ν_e) scales linearly with the integrated "hot-spot" signal strength. This pseudoband can be used to calibrate "hot spot" variations and minimize the signal heterogeneity of a SERS substrate, account for batch-to-batch substrate variability and different types of SERS substrates. We first discuss the fundamental theory supporting our approach, provide supporting experimental results, and conclude by demonstrating "hot spot" normalization for (1) quantitative pH-triggered SERS detection of chloroanilines and (2) differentiation of analyte adsorption and "hot spot" formation in a dynamic colloidal system.

DOI: 10.1021/acs.analchem.7b04667
Anal. Chem. 2018, 90, 3227−3237

EXPERIMENTAL SECTION

Materials. Gold(III) chloride trihydrate ($HAuCl_4 \cdot 3H_2O$), sodium citrate tribasic dehydrate ($Na_3Cit \cdot 2H_2O$), silver nitrate ($AgNO_3$), 4-chloroaniline (4-CA, 98%), 3-chloroaniline (3-CA, 99%), 2-chloroaniline (2-CA, 98%), 2,4-dichloroaniline (99%), 3-bromoaniline (3-BA), 3-nitroaniline (3-NA), melamine, and 4-mercaptobenzoic acid (4-MBA) were purchased from Sigma-Aldrich. Sodium borohydride ($NaBH_4$), hydrochloride acid (HCl), and ethanol were purchased from Fisher Scientific. Malachite green isothiocyanate (MGITC) was acquired from Invitrogen Corp. (Grand Island, NY). Thiolated poly(ethylene glycol) (HS-PEG; 5 kDa) was purchased from Nanocs.

Transmission Measurement. SERS spectra of DI water were collected using a transmission mode Raman system equipped with an inverted microscope (WITec alpha 300 RSA +). Two identical objectives were used (20×, NA = 0.4) to focus into the sample with a spot size of ≈2.4 μm and collect the signal through the sample. The laser excitation wavelength was 785 nm. We employed a long-pass filter (cutoff wavelength: 68 cm^{-1}) before the detector to generate pseudoband ν_e, and a bandpass filter (center wavelength: 785 nm, Full Width-Half Max: 3 nm) was placed to block the elastic scattering process of ASE fields from the laser. Before the laser and detector, there were two small confocal pinhole apertures that increase optical resolution and suppress out-of-focus light.

Backscattering Measurement. All SERS spectra except the laser emission profile shown in Figure 1c were acquired using a confocal Raman spectroscopy system in backscattering mode (WITec alpha 500R). SERS maps were generally collected with a 10× objective. Each SERS map consists of 20 × 20 spectra across a 100 × 100 μm^2 area. The laser wavelength was 785 nm and integration time was 0.5 s. The Raman signal was dispersed by a 300 gr/mm grating and detected using a Peltier charge-coupled device. To make HS normalized maps, spectra from a SERS map were imported into Matlab 2015 (The Mathworks, U.S.A.) and baseline corrected using in-house scripts. For the maps using PL as normalizing factor, only the dark background (Figure 1e) was subtracted. As shown in Figure S1, the Au−Cl Raman band at 267 cm^{-1} does not influence ν_e even when an edge filter cutting at 126 cm^{-1} was employed. Integrated intensities from 106 to 146 cm^{-1} for ν_e at 126 cm^{-1} or 64−104 cm^{-1} for ν_e at 84 cm^{-1} were employed as the normalizing factor. The ratio of the analyte band to ν_e was projected as a normalized SERS map using Matlab.

Preparation of SERS Substrates. Preparation and characterization of the AuNP/BC platform was described previously.[7] Briefly, 16 pieces of BC (0.5 cm × 0.5 cm) were immersed in 0.7 mL $HAuCl_4$ solution (30 mM) for 30 s and then transferred to 50 mL boiling Na_3Cit solution (1.2 mM unless otherwise denoted) for 1.5 h. Scanning electron microscopy images, energy dispersive X-ray spectroscopy, and UV−vis extinction spectra are shown in Figures S2 and S3 and in our previous publication.[7] AgNP/BC was prepared by adding 0.7 mL of $NaBH_4$ (25 mM unless otherwise denoted) into a tube containing 0.7 mL of $AgNO_3$ (25 mM) and 20 pieces of BC followed by vortex mixing. The preparation method for 14 nm AuNP seeds and 50 nm AuNPs is described in Supporting Information Note S1. Briefly, AuNP seeds were synthesized by adding Na_3Cit solution (final concn: 3.88 mM) to boiling $HAuCl_4$ solution (final concn: 1 mM) for 15 min. AuNPs (50 nm) were synthesized by seed-mediated growth. A 100 mL $HAuCl_4$ solution (final concn: 0.254 mM) was brought to boil, to which 0.818 mL of seed solution and 0.44 mL of citrate (38.8 mM) were subsequently added. 4-MBA coated AuNP aggregate suspension was prepared by ethanol-induced aggregation followed by thiolated poly(ethylene) glycol (HS-PEG) functionalization.[28]

Manipulation of Hot Spot Density in AuNP/BC Substrate. One piece of AuNP/BC (0.5 × 0.5 cm^2) hydrogel was immersed in 5 mL of 4-MBA ethanol solution (1 mM) for 3 h. The 4-MBA concentration used here was high enough to ensure that a complete monolayer formed on the nanoparticle surface. SERS maps were collected from the wet AuNP/BC hydrogel in air every 20 min until 60 min. After the AuNP/BC was completely dry, SERS maps were collected using both 10× and 100× objectives.

pH-Triggered Detection of Four Chloroanilines. Sample aliquots of 1 mL of 4-CA, 3-CA, 2-CA, or 2,4-DCA in ethanol solutions with a concentration of 1 mM were added to 3 mL aqueous solution with pH preadjusted to values below their pK_a. The final ethanol concentration (25%) had minimal influence on SERS detection (data not shown). One piece of AuNP/BC (0.5 × 0.5 cm^2) hydrogel was immersed in chloroaniline solution. After vortex mixing for 30 s, the AuNP/BC hydrogel was taken out for SERS measurement.

Quantitation of Chloroanilines. To determine the dynamic range of four chloroanilines, 1 mL 4-CA, 3-CA, 2-CA, and 2,4-DCA in ethanol with concentrations from 1 to 1000 μM was added to a 3 mL aqueous solution with pH preadjusted to 1.7−2.3. One piece of AuNP/BC (0.5 × 0.5 cm^2) hydrogel was immersed in the chloroaniline solution. After vortex mixing for 30 s, the AuNP/BC hydrogel was taken out for Raman measurement.

SERS Spectra Collection with a Variety of Analytes and Substrates. SERS spectra of a variety of analytes were acquired using an AuNP/BC platform via a pH-triggered approach.[7] In this process, 1 mL of analyte in ethanol (1 mM) was added to a 3 mL aqueous solution of preadjusted pH to ensure that solution pH values were below the analyte pK_a. The final pH values were: MGITC: 5.4; 4-CA: 2.3; 3-CA: 1.9; 2-CA: 1.9; 2,4-DCA: 1.7; Melamine: 2.3; 3-BA: 2.3; and 3-NA: 1.8. One piece of AuNP/BC (0.5 × 0.5 cm^2) hydrogel was immersed in each solution. After vortex mixing for 30 s, the AuNP/BC hydrogel was taken out for Raman measurement. SERS spectra of blank AuNP/BC were collected at pH values of 5.4 and 2.3 as negative controls.

Monitoring 4-MBA Adsorption to Stable and Dynamic SERS Substrates. A piece of AuNP/BC was attached to the bottom of a small Petri dish. After collecting the first SERS map (blank), 6 mL of 4-MBA ethanol/water solution (50 μM) was added. SERS spectra were collected every 1 min for the first five spectra, every 5 min for the next five spectra, every 10 min for the next five spectra, and every 20 min for the remaining four spectra. To monitor 4-MBA adsorption to aggregating AuNP surface, 0.5 mL of 4-MBA ethanol solution (100 μM) was added into 0.5 mL of AuNP suspension. After the mixture was mixed by vortexing, it was transferred to a quartz cell and scanned. SERS maps (20 × 20 points, 1000 × 1000 μm^2, 0.5 s int. time) were collected every 5 min until 180 min. Before calculating the ratio between the Raman and elastic bands, the blank spectrum was subtracted from each SERS spectrum to exclude the influence of ASE photons scattered by water.

DOI: 10.1021/acs.analchem.7b04667
Anal. Chem. 2018, 90, 3227−3237

RESULTS AND DISCUSSION

Theoretical Basis for "Hot Spot" Normalization. Using a scalar phenomenological theory,[29,30] we developed an analytical expression that predicts that the intensity of the surface-enhanced elastic scattering signal is proportional to the SERS signal from the ensemble of analyte and background molecules in the vicinity of plasmonic nanostructures. We propose that the surface-enhanced elastic scattering signal can serve as an intrinsic internal standard for quantitative SERS under carefully controlled conditions.

As depicted in Figure 1a, a molecule is located at position r_0 close to a plasmonic metal nanostructure (at r′) that supports localized surface plasmon resonances (LSPRs) and converts the incident fields $E_0(r_0, \omega_0)$ into local scattered fields $E_R(r_0, \omega_0) \sim f(r_0, \omega_0)E_0(r_0, \omega_0)$, where $f(r_0, \omega_0)$ is the field enhancement factor. Laser illumination gives rise not only to the stimulated emission fields $E_0(r_0, \omega_0)$ at the lasing frequency ω_0, but also amplified spontaneous emission (ASE) fields $E_0(r_0, \omega_1)$ over broad frequencies ω_1 that have weaker amplitudes than the lasing emission. An analyte molecule at r_0 experiences the total local fields $E_0 + E_s \sim (1+f(r_0, \omega))^*E_0(r_0, \omega)$ at lasing frequency ω_0 and ASE frequencies ω_1, respectively. The interaction of the molecule with the enhanced total local fields at ω_0 gives rise to the dipole moment associated with inelastic Raman scattering according to $p(\omega_0 \pm \omega_{vib}, \omega_0) = \alpha(\omega_0 \pm \omega_{vib}, \omega_0)[1 + f(r_0, \omega_0)]E_0(r_0, \omega_0)$, where ω_{vib} is a vibrationally shifted frequency and $\alpha(\omega_0 \pm \omega_{vib}, \omega_0)$ is the polarizability for the frequency mixing Stokes (ω_0 - ω_{vib}) or anti-Stokes (ω_0 + ω_{vib}) Raman scattering process. Similarly, the dipole moment associated with elastic scattering at frequency ω_1 can be induced according to $p(\omega_1) = \alpha(\omega_1)[1 + f(r_0, \omega_1)]E_0(r_0, \omega_1)$, where $\alpha(\omega_1)$ is the polarizability of the elastic scattering process. In the presence of plasmonic nanostructures, the Green function $G(r_\infty, r_0, \omega)$ of the combined molecule-nanostructure system is represented as $(1+f(r_0, \omega))\, G_0(r_\infty, r_0, \omega)$, where G_0 is the free-space Green function in the absence of plasmonic nanostructures and f is the field enhancement factor at the radiation frequency. The electric field intensity I_{Raman} of the radiation from the induced Raman scattering dipole $p(\omega_0 \pm \omega_{vib}, \omega_0)$ depends on the incident field intensity I_0 and can be expressed as

$$
\begin{aligned}
I_{\mathrm{Raman}}(r_\infty, \omega_0 \pm \omega_{\mathrm{vib}}) &= |E(r_\infty, \omega_0 \pm \omega_{\mathrm{vib}})|^2 \\
&= \left|\frac{(\omega_0 \pm \omega_{\mathrm{vib}})^2}{\varepsilon c^2}[G(r_\infty, r_0, \omega_0 \pm \omega_{\mathrm{vib}})]p(\omega_0 \pm \omega_{\mathrm{vib}}, \omega_0)\right|^2 \\
&\approx \frac{(\omega_0 \pm \omega_{\mathrm{vib}})^4}{\varepsilon^2 c^4}\left|[1 + f(r_0, \omega_0 \pm \omega_{\mathrm{vib}})]G_0(r_\infty, r_0, \omega_0 \pm \omega_{\mathrm{vib}})\right. \\
&\quad \left.\alpha(\omega_0 \pm \omega_{\mathrm{vib}}, \omega_0)[1 + f(r_0, \omega_0)]\right|^2 I_0(r_0, \omega_0)
\end{aligned} \tag{1}
$$

Similarly, the radiation intensity I_{Elastic} from the induced elastic scattering dipole $p(\omega_1)$ is

$$
\begin{aligned}
I_{\mathrm{Elastic}}(r_\infty, \omega_1) &= |E(r_\infty, \omega_1)|^2 \\
&= \left|\frac{\omega_1^2}{\varepsilon c^2}[G_0(\vec{r_\infty}, \vec{r_0}, \omega_1) + G_R(\vec{r_\infty}, \vec{r_0}, \omega_1)]p(\omega_1)\right|^2 \\
&\approx \frac{\omega_1^4}{\varepsilon^2 c^4}\left|[1 + f(r_0, \omega_1)]G_0(r_\infty, r_0, \omega_1)\alpha(\omega_1)[1 + f(r_0, \omega_1)]\right|^2 I_0(r_0, \omega_1)
\end{aligned} \tag{2}
$$

For most quantitative SERS applications, we want to quantify analyte molecule concentrations by measuring Raman signals from an ensemble of analyte molecules in a dielectric environment (e.g., various liquids). Under laser illumination both the inelastic Raman scattering and the elastic scattering signals come from an ensemble of analyte and background molecules. According to eq 1 and eq 2, the ratio of signal intensities between Raman scattering at $\omega_0 \pm \omega_{\mathrm{vib}}$ and elastic scattering at ω_1 can be expressed as

$$
\begin{aligned}
\frac{I_{Raman}(r_\infty,\omega_0\pm\omega_{vib})}{I_{Elastic}(r_\infty,\omega_1)} &= \frac{\sum_{i=1}^{N_A V} I^i_{Raman}(r_\infty,r^i_0,\omega_0\pm\omega_{vib})}{\sum_{i=1}^{N_A V} I^i_{Elastic}(r_\infty,r^i_0,\omega_1)+\sum_{j=1}^{N_B V} I^j_{Elastic}(r_\infty,r^j_0,\omega_1)} \approx \frac{\sum_{i=1}^{N_A V} I^i_{Raman}(r_\infty,r^i_0,\omega_0\pm\omega_{vib})}{\sum_{j=1}^{N_B V} I^j_{Elastics}(r_\infty,r^j_0,\omega_1)} \\
&= \frac{\sum_{i=1}^{N_A V}\left|G_0(r_\infty,r^i_0,\omega_0\pm\omega_{vib})\alpha_A(\omega_0\pm\omega_{vib},\omega_0)f(r^i_0,\omega_0\pm\omega_{vib})f(r^i_0,\omega_0)\right|^2 I_0(r^i_0,\omega_0)}{\sum_{j=1}^{N_B V}\left|G_0(r_\infty,r^j_0,\omega_1)\alpha_B(\omega_1)\left[f(r^j_0,\omega_1)\right]^2\right|^2 I_0(r^j_0,\omega_1)}.
\end{aligned} \tag{3}
$$

where N_A, N_B are the molar concentrations of the analyte and the background solvent molecules ($N_B \gg N_A$) present within the sampling volume V, $\alpha_A(\omega_0 \pm \omega_{vib}, \omega_0)$ is the Raman scattering polarizability of the analyte molecules, $\alpha_B(\omega_1)$ is the elastic scattering polarizability of the background molecules, and r^i_0, r^j_0 are the positions of analyte molecule i and background molecule j.

If we constrain the optical sampling volume within a tightly focused spot that contains plasmonic nanostructures (e.g., by use of a confocal configuration), both the surface-enhanced elastic scattering and the inelastic scattering signals will be dominated by the analyte and background molecules located in close proximity to "hot spots" that induce the maximum intensities of both elastic and inelastic scattering proportional to $|f_{max}|$,[4] where f_{max} is the maximum field enhancement factor in the hot spot region at the excitation frequency ω_0.[27] Because $\omega_0 \cong \omega_1 \gg \omega_{vib}$, we assume $f_{max}(r_0, \omega_0) \cong f_{max}(r_0, \omega_1) \cong f_{max}(r_0, \omega_0 \pm \omega_{vib}) \equiv f_{max} \gg 1$, and $G_0(r_\infty, r_0, \omega_1) \cong G_0(r_\infty, r_0, \omega_0 \pm \omega_{vib})$. In this case, the ratio of Raman and elastic signal intensities can be approximated as

$$
\begin{aligned}
&\frac{I_{\mathrm{Raman}}(r_\infty, \omega_0 \pm \omega_{\mathrm{vib}})}{I_{\mathrm{Elastic}}(r_\infty, \omega_1)} \\
&\approx \frac{N_A |G_0(r_\infty, r_0, \omega_0 \pm \omega_{\mathrm{vib}})\alpha_A(\omega_0 \pm \omega_{\mathrm{vib}}, \omega_0)[f_{\max}]^2|^2 I_0(r_0, \omega_0)}{N_B |G_0(r_\infty, r_0, \omega_1)\alpha_B(\omega_1)[f_{\max}]^2|^2 I_0(r_0, \omega_1)} \\
&\approx \frac{N_A |\alpha_A(\omega_0 \pm \omega_{\mathrm{vib}}, \omega_0)|^2 I_0(r_0, \omega_0)}{N_B |\alpha_B(\omega_1)|^2 I_0(r_0, \omega_1)}
\end{aligned} \tag{4}
$$

During a SERS measurement, all factors (e.g., N_B, α_A, α_B, and $I_0(r_0, \omega_0)/I_0(r_0, \omega_1)$) except N_A in eq 4 are constant. By normalizing the SERS signals with the surface-enhanced elastic scattering signals of the background molecules in the "hot spots", the new ratiometric signal, $\frac{I_{\mathrm{Raman}}(r_\infty, \omega_0 \pm \omega_{\mathrm{vib}})}{I_{\mathrm{Elastic}}(r_\infty, \omega_1)}$, provides

DOI: 10.1021/acs.analchem.7b04667
Anal. Chem. 2018, 90, 3227−3237

quantitation of the molar concentration of analyte molecules N_A without being affected by the many experimental factors that give rise to uncontrollable spatial and temporal perturbations (e.g., local refractive index environments, local field enhancement factors, and local laser illumination fluxes).

We emphasize that the elastic scattering polarizability $\alpha_B(\omega_1)$ is many orders larger than the Raman scattering polarizability $\alpha_A(\omega_0 \pm \omega_{vib}, \omega_0)$ and that N_B is generally orders of magnitude higher than N_A. Consequently, to maintain a large signal-to-noise for quantitative SERS applications, we must ensure that $I_0(r_0, \omega_0)$ (=excitation field intensity for Raman scattering) ≫ $I_0(r_0, \omega_1)$ (=excitation field intensity for elastic scattering) in eq 4. This condition can be satisfied by using intense lasing light and weak ASE light in the laser emission.

Origin of ν_e. As a proof of concept, we used a confocal Raman microspectroscopy/imaging setup (Figure 1b) to simultaneously collect and compare inelastic Raman and elastic scattering signals from a tightly focused spot on a nanostructured plasmonic substrate. As shown in Figure 1c, the measured diode laser (785 nm) emission spectrum (red curve) consists of a narrow laser line at 0 cm^{-1} along with a broad ASE background that extends beyond 200 cm^{-1}. After blocking the laser emission with a long-pass (edge) filter, we observe an asymmetric peak (ν_e) at 76 cm^{-1} that is an artificial/pseudo spectral feature due to the convolution of the spectral profile of the ASE and the transmittance of the filter (cut-on wavenumber: 68 cm^{-1}). By choosing long-pass filters with different cut-on wavenumbers and cutoff slopes, we can control the spectral position, shape, and amplitude of ν_e (Figure S4). For instance, when we insert a bandpass filter in addition to the long-pass filter, the pseudo peak (ν_e) at 76 cm^{-1} (green curve) is significantly attenuated showing that ν_e originates from the laser ASE.

Because ν_e is weak, it has been typically overlooked based on the assumption that elastic scattering will be fully blocked by the long-pass filter.[31,32] This assumption deviates from the reality of many SERS studies. We speculated that the weak ν_e interacts with SERS "hot spots", is elastically scattered by the molecules within them and experiences the same electromagnetic enhancement as Raman scattering.[27] To test this hypothesis, backscattered Raman spectra of a Si wafer and a SERS substrate, that is, gold nanoparticle/bacterial cellulose (AuNP/BC), were collected. As shown in Figure 1d, an asymmetric peak at 76 cm^{-1} appears in the Raman spectra for both Si and the SERS substrate that reflects the line shape of the laser ASE (red curve). Notably, the ν_e of AuNP/BC was 2600× larger than that of the Si wafer, thus supporting the hypothesis that ν_e is significantly enhanced by SERS "hot spots" (Figure 1d).

As shown in Figure S5 and Note S2, additional experiments using a second Raman instrument equipped with an edge filter (cut-on wavenumber: 126 cm^{-1}) to probe AuNP/BC, a commercial SERS substrate, and aggregated AuNP colloids corroborate this result. AuNP monomer colloid exhibited an extremely weak ν_e, which was almost identical to that of DI water. ν_e was significantly enhanced following the addition of phosphate buffer to the colloid, concomitant to hot spot formation (Figure S5). The intensities of ν_e ($I_{Elastic}(r_\infty, \omega_1)$) of AuNP/BC (high hot spot density), AuNP cluster colloid (low hot spot density), AuNP monomer colloid (no hot spots), and DI water (no hot spots) followed the trend: DI ≈ AuNP monomer < AuNP cluster < AuNP/BC at any given incident laser power (Figure S6). Across all experiments, ν_e is characteristically weak in the absence of large numbers of SERS hotspots. Therefore, we neglected the contribution of molecules and nanoparticles located outside hot spots to ν_e in the following discussion.

We emphasize that ν_e occurs in addition to the SERS background continuum that originates from the combination of the photoluminescence (PL) of the plasmonic nanostructures and the fluorescence emitted by fluorophores near the surface under laser excitation.[33−36] Fluorophores in resonance with the excitation laser are subject to surface-enhanced fluorescence (SEF) that contributes to the background continuum.[35,37,38] To minimize this possibility, we primarily used a nonresonant molecule, 4-MBA, and thoroughly washed our substrates such that residual fluorophores were removed. PL originates from the radiative recombination of sp band electrons and excited d band holes in noble metals and can be significantly enhanced by the surface plasmon resonance of nanostructures.[32,36,39] PL is an inherent characteristic of the SERS spectrum and is typically the primary contributor to the SERS continuum. Many SERS studies report spectra in a range far away from the excitation wavelength (>200 cm^{-1})[37,40,41] where the PL signal can dominate the SERS continuum. It should be noted, however, that for any given SERS substrate the contribution of PL to the SERS continuum will be a function of the laser excitation wavelength.[32,40] To illustrate, the AuNP/BC substrate was probed using both 633 and 785 nm excitation. As shown in Figure 1e, the PL background of the SERS spectrum obtained with the 633 nm laser perfectly predicts the PL background of the SERS spectrum collected under 785 nm excitation. The contribution of PL to the pseudopeak at 84 cm^{-1} (the red-shaded areas) is a function of the laser excitation, with a larger contribution under 633 nm excitation (∼50.1%) than at 785 nm (∼6.5%). Figure 1e illustrates the additive contribution of surface-enhanced elastic scattering to ν_e relative to the broad, smooth PL background.[36] The influence of PL on the intensity of ν_e is readily accounted for by baseline correction using published Matlab scripts (Figure S7).[42]

The strong correlation between PL and the dark-field scattering spectra of individual plasmonic nanoparticles/clusters demonstrates that the PL spectrum is dependent on the localized surface plasmon resonance (LSPR) of the nanostructures.[32,34,36,43,44] This LSPR dependence was experimentally demonstrated by the dissimilar SERS backgrounds of two SERS substrates, AgNP/BC and AuNP/BC, for wavenumbers >188 cm^{-1} where the laser ASE is quite weak (Figure 1d, Figure S8). The ν_e line shapes for these substrates overlap and resemble the line shape of the laser ASE < 188 cm^{-1} (Figure 1d), further indicating that ν_e originates from ASE and not PL.

Figure 1f shows the Raman spectra of 4-mercaptobenzoic acid (4-MBA) functionalized AuNP clusters under various laser powers. The intensities of the laser band (0 cm^{-1}), the elastic pseudo peak (126 cm^{-1}), and the most intense Raman bands (1076 and 1587 cm^{-1}) are plotted in Figure 1g. Each of these bands increase linearly with an increase in laser power. As expected based on our theoretical analysis, the intensity trend for the pseudo elastic scattering peak is similar to that of the Raman bands. The intensity of ν_e at 126 cm^{-1} is of comparable magnitude to the Raman scatting intensity, which makes it a potentially suitable internal standard for calibration of the SERS signals. To validate this hypothesis the intensity ratios of the pseudo peak (126 cm^{-1}) and two Raman bands (1076 and 1587 cm^{-1}) are plotted in Figure 1h. These ratios are independent of laser intensity, a finding in agreement with eq 4.

DOI: 10.1021/acs.analchem.7b04667
Anal. Chem. 2018, 90, 3227−3237

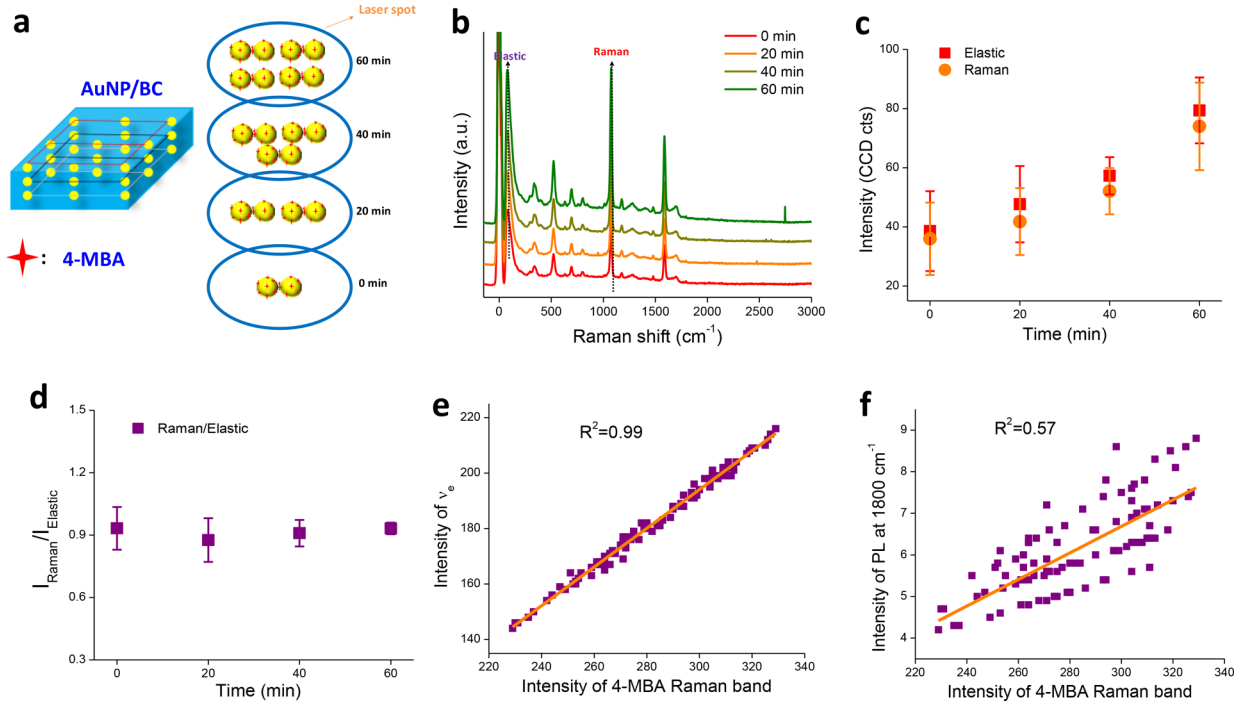

Figure 2. (a) Schematic of the increase in SERS "hot spot" density within the laser excitation volume that occurs due to AuNP/BC hydrogel drying; (b) The Raman spectra of 4-MBA on AuNP/BC platform at different drying times; The intensity of the Raman band at 1076 cm^{-1} of 4-MBA as the AuNP/BC hydrogel was drying (c) before and (d) after HS normalization; Variation of the SERS intensity of the 4-MBA Raman band at 1076 cm^{-1} as a function of the intensity of the (e) elastic band at 84 cm^{-1} and (f) photoluminescence (PL) background at 1800 cm^{-1} across a SERS map acquired on the AuNP/BC platform (100 points were randomly selected from a SERS map containing 400 pixels).

Reducing SERS Substrate Heterogeneity by HS Normalization. All other parameters being fixed, the ratio defined by eq 4 will be constant no matter how "hot spot" density changes. To illustrate, we exploited an AuNP/BC hydrogel[7] that exhibits temporally variable "hot spot" densities as a function of drying time (Figure 2a). Over a 1 h drying period, both the 4-MBA Raman band at 1076 cm^{-1} and ν_e increase in intensity due to the drying mediated increase in "hot spot" density (Figure 2b,c). Despite these temporal changes, however, the ratio between the Raman band and ν_e remained constant (Figure 2d), as expected.

We suggest that the intensity of ν_e provides an indication of the integrated strength of SERS efficiency from all "hot spots" within the microscope collection volume. One hundred spectra were randomly selected from a 400 pixel SERS map of 4-MBA on AuNP/BC. Across this map, as shown in Figure 2e, the intensity of the 4-MBA Raman band at 1076 cm^{-1} increased linearly with the intensity of ν_e ($R^2 = 0.99$). This linearity shows that ν_e quantitatively reflects the integrated SERS efficiency of the excited "hot spots". We note that the intensity of the 4-MBA Raman band correlates poorly with the intensity of the PL background (Figure 2f), thus indicating that ν_e can serve as a SERS internal standard while the SERS continuum cannot.

The measured SERS intensity of any analyte reflects the combined effects of laser intensity, the electromagnetic field within SERS "hot spots", "hot spot" density, and the number of analyte molecules within the probe volume.[45] As discussed previously, the fluctuations of the first three factors are significantly reduced by ν_e normalization, leaving the number of analyte molecules as the remaining variable dictating signal intensity. Normalization by ν_e ($= I_{Raman}/I_{Elastic}$) decreases the variability of the SERS signal by minimizing point-to-point variations in SERS "hot spot" densities. We refer to this approach as "hot spot" (HS) normalization.

HS normalization significantly reduces the point-to-point heterogeneity of SERS substrates. Using the AuNP/BC substrate and 4-MBA as our test analyte, Raman maps (100 × 100 μm^2; 400 pixels) were constructed by separately tracking the Raman band at 1076 cm^{-1}, ν_e at 84 cm^{-1}, and background PL at 1820 cm^{-1} (Figure 3a–j). The maps tracking the Raman band and ν_e exhibit highly similar "hot spot" distributions illustrating that Raman scattering and elastic scattering are similarly enhanced. The measured coefficients of variation (CV), or the ratio of the standard deviation to the mean, were 9.3 and 18.8% for the 10× and 100× objectives, respectively. However, following HS normalization, the CVs declined to 2.3 and 7.9%, respectively. After HS normalization, all the "hot spots" and "cold spots" (i.e., spots with below average signal intensity) disappear, graphically illustrating the concept of HS normalization. Averaging SERS signals across a map can also reduce signal fluctuation.[46] However, the "averaging" approach sacrifices the spatial resolution of SERS, is time consuming, and may not work well for substrates with low hot spot density.

Recently, Ren et al. retrieved the original relative intensity among Raman bands by normalizing SERS spectra by the scattering spectra of the same nanoparticles (or bulk material photoluminescence (PL_{bulk})-normalized SERS background).[34] The aim of their study was to mitigate the plasmonic spectral shaping effect caused by varying nanoparticle LSPRs, whereas our aim was to reduce the SERS signal fluctuation caused by varying electromagnetic enhancements. In addition, the approach proposed by Ren et al. was more time-consuming because of the requirement for collecting PL_{bulk} and the more complex data analysis. Maps normalized using background PL exhibit little improvement in CV. The differential performance

DOI: 10.1021/acs.analchem.7b04667
Anal. Chem. 2018, 90, 3227–3237

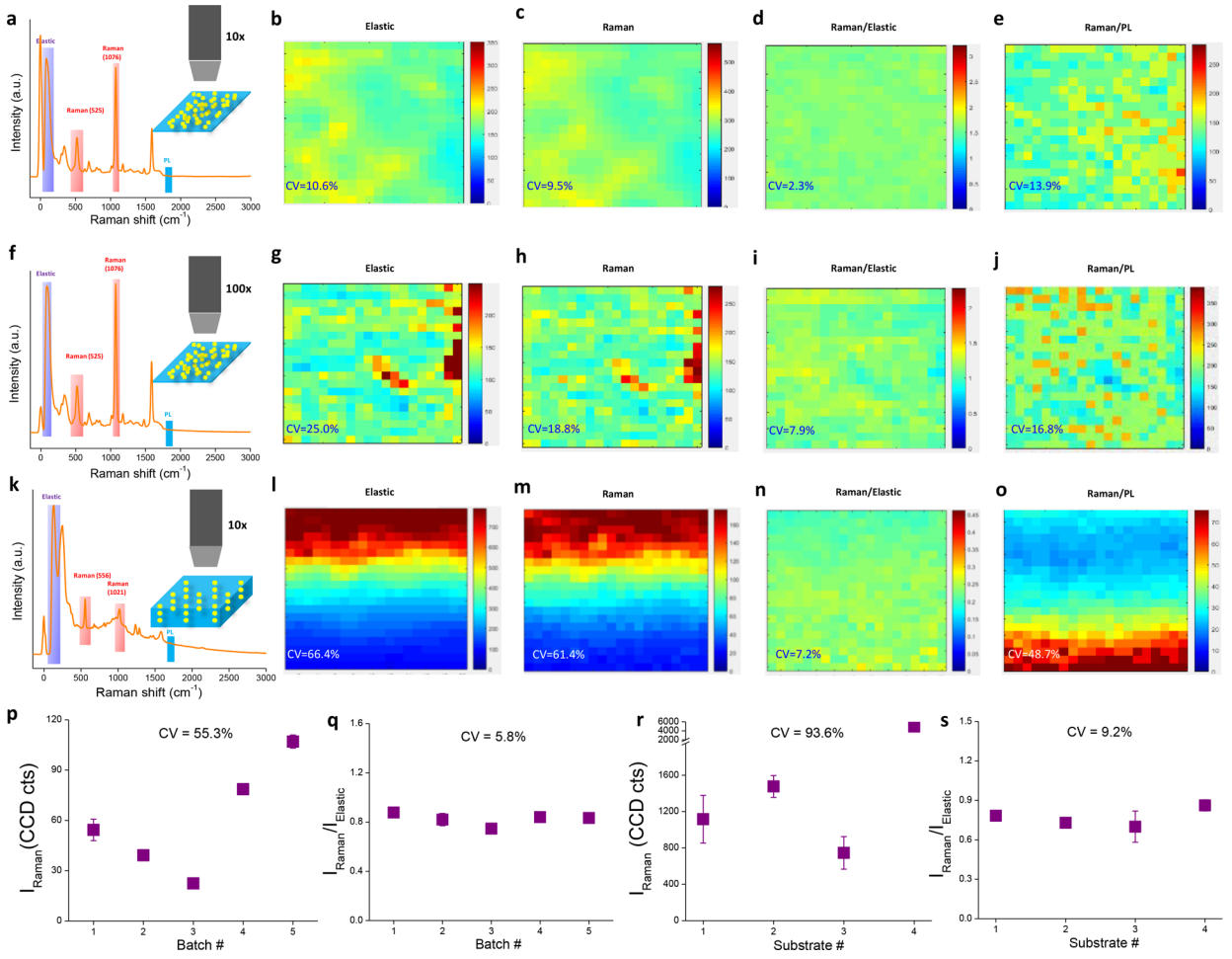

Figure 3. SERS spectra and maps of 4-MBA on dry AuNP/BC film collected using 10× (a–e) and 100× (f–j) objectives. Maps of 4-MBA tracking the bands at 84 cm^{-1} (b), 1076 cm^{-1} (c), the ratio between the two bands (I_{1076}/I_{184}) (d), the ratio between the band at 1076 cm^{-1} and the PL background (I_{1076}/I_{1820}) (e). Maps of 4-MBA tracking the bands at 84 cm^{-1} (g), 1076 cm^{-1} (h), the ratio between the two bands (I_{1076}/I_{84}) (i), and the ratio between the band at 1076 cm^{-1} and the PL background (I_{1076}/I_{1820}) (j). Maps of 2-CA from a drying AuNP/BC hydrogel tracking the bands at 126 cm^{-1} (l), 556 cm^{-1} (m), the ratio between the two bands (I_{556}/I_{126}) (n), and the ratio between the band at 556 cm^{-1} and the PL background (I_{556}/I_{1820}) (o). All maps were collected across a 100 μm × 100 μm area and contained 400 single spectra. (p) SERS signals of 4-MBA Raman band at 1076 cm^{-1} collected from AuNP/BC substrates prepared by three different people and in five batches; (q) The HS normalized (I_{1076}/I_{84}) signal for 4-MBA collected from AuNP/BC substrates prepared in five batches; (r) SERS signals of 4-MBA Raman band at 1076 cm^{-1} collected using four different SERS substrates; (s) The ratio between the two bands (I_{1076}/I_{84}) of 4-MBA collected using four different SERS substrates. Substrates #1 and #2 are AuNP/BC nanocomposites prepared using 1.2 mM or 12 mM Na_3Cit as reducing agent, respectively; Substrates #3 and #4 are AgNP/BC nanocomposites prepared using 250 mM or 25 mM $NaBH_4$ as reducing agent, respectively; Each substrate was scanned (containing 400 pixels) three times, and the error bars reflect the standard deviation of these three scans.

of PL vs ν_e as a SERS internal standard is attributed to their different enhancement mechanisms. PL reflects the enhancement of a radiating dipole comprising d-bands and s-electrons in the presence of a LSPR.[47] In contrast, ν_e is enhanced by the same electromagnetic mechanism responsible for SERS.[27] No correlation was observed between the elastic band at laser excitation wavenumber (0 cm^{-1}) and Raman band, which was consistent with the literature.[48] The mechanism for the distinct behaviors of laser band at 0 cm^{-1} and ν_e is our research interest in the future. The concept of HS normalization is extendable to other 4-MBA Raman bands as well as AuNP suspension-based SERS (Figures S9–11). It is notable that the number of hot spots within the excitation volume for the AuNP cluster colloid was estimated to be ≈1,[28] indicating that HS normalization reduced the HS-to-HS fluctuation of SERS signals (Figures S10,11). HS normalization is possible with ν_e pseudopeaks set using a range of long-pass filters (Figure S11) and variable sampling areas (Figure S12).

Finally, HS normalization can account for batch-to-batch variability in substrate performance (Figure 3p,q) as well as differences in substrate identity (Figure 3r,s). To illustrate, five batches of AuNP/BC were prepared by three separate individuals and scanned after exposure to 50 μM 4-MBA for 2 h. The CV value of the Raman band at 1076 cm^{-1} of 4-MBA decreased from 55.3% to 5.8% after HS normalization (Figure 3p,q), indicating that HS normalization can significantly improve batch-to-batch reproducibility of SERS substrates. Four nanocellulose-based SERS substrates prepared using two different metals (Au or Ag) and two different reducing agents (NaCit or $NaBH_4$) were scanned by Raman after exposing to 50 μM 4-MBA for 2 h. The LSPR of a nanostructure is an important parameter influencing its SERS enhancement factor.[49] The four substrates exhibited different extinction

DOI: 10.1021/acs.analchem.7b04667
Anal. Chem. 2018, 90, 3227–3237

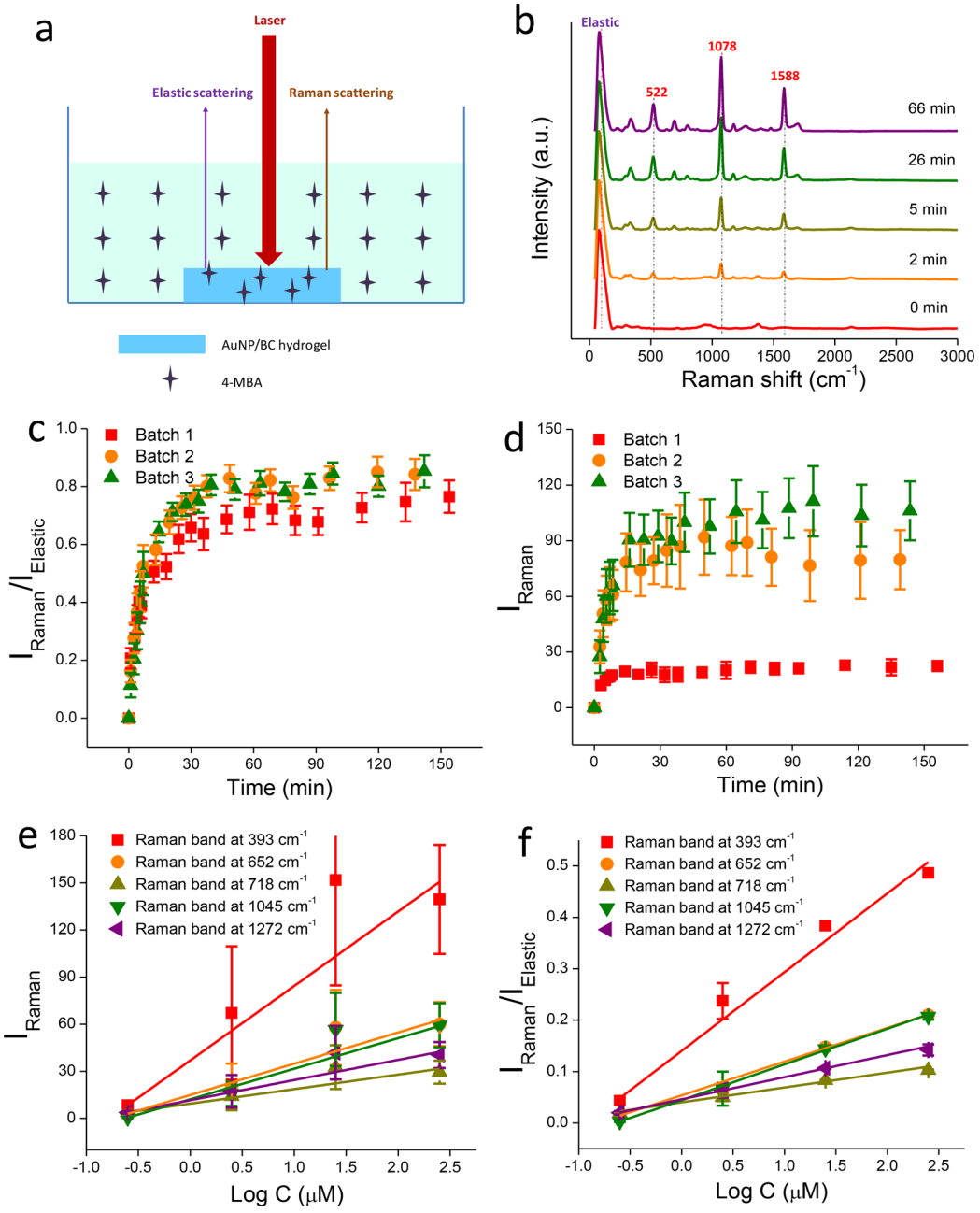

Figure 4. (a) Schematic of the experimental setup for monitoring 4-MBA adsorption kinetics onto AuNP/BC. (b) Selected SERS spectra of 4-MBA collected on AuNP/BC at different time after adding 4-MBA. (c) Variation of the ratio between the Raman band at 1076 cm^{-1} and ν_e at 84 cm^{-1} as a function of time. (d) Variation of the Raman band at 1076 cm^{-1} as a function of time. (e) Variation of non-normalized SERS intensities of 2,4-DCA as a function of their logarithmic concentrations. (f) Variation of normalized SERS intensities of 2,4-DCA as a function of their logarithmic concentrations. Error bars reflect the standard deviation of SERS intensities from three collected average spectra. Each average spectrum is the average of 400 spectra in a 100 μm × 100 μm SERS map.

spectra (Figure S13). The intensities of the Raman bands and ν_e collected from the four substrates varied simultaneously (Figure S14), indicating their LSPRs exerted the same influence on both types of bands. The CV value of the 1076 cm^{-1} Raman band decreased from 93.6% to 9.2% after HS normalization (Figure 3r,s), indicating that HS normalization can significantly improve the reproducibility across a suite of different SERS substrates.

Our measured CV value of 2.3% is, to the best of our knowledge, the lowest reported in the literature (Table S2). Such a result is impressive given that the AuNP/BC substrate is heterogeneous with respect to nanoparticle size, shape, and aggregation state and thus the numbers of 4-MBA molecules associated with any given "hot spot" (N_A) will not be 100% identical across the map. Most approaches to achieve low CV values rely on expensive lithographic techniques or apply highly specialized analyte dosing or added internal standards.[17,50,51] As shown in Table S2, Sepaniak et al. produced a highly homogeneous SERS substrate by electron beam lithography and nanotransfer printing that exhibited a CV value of 13%.[10] Similarly, well-patterned gold nanocluster arrays fabricated via template-guided self-assembly exhibited a CV value of 12%.[52] Most recently, Chen et al. achieved a then record-low CV value (4.3%) by "fixing" analytes in a "hot zone" above an

DOI: 10.1021/acs.analchem.7b04667
Anal. Chem. 2018, 90, 3227−3237

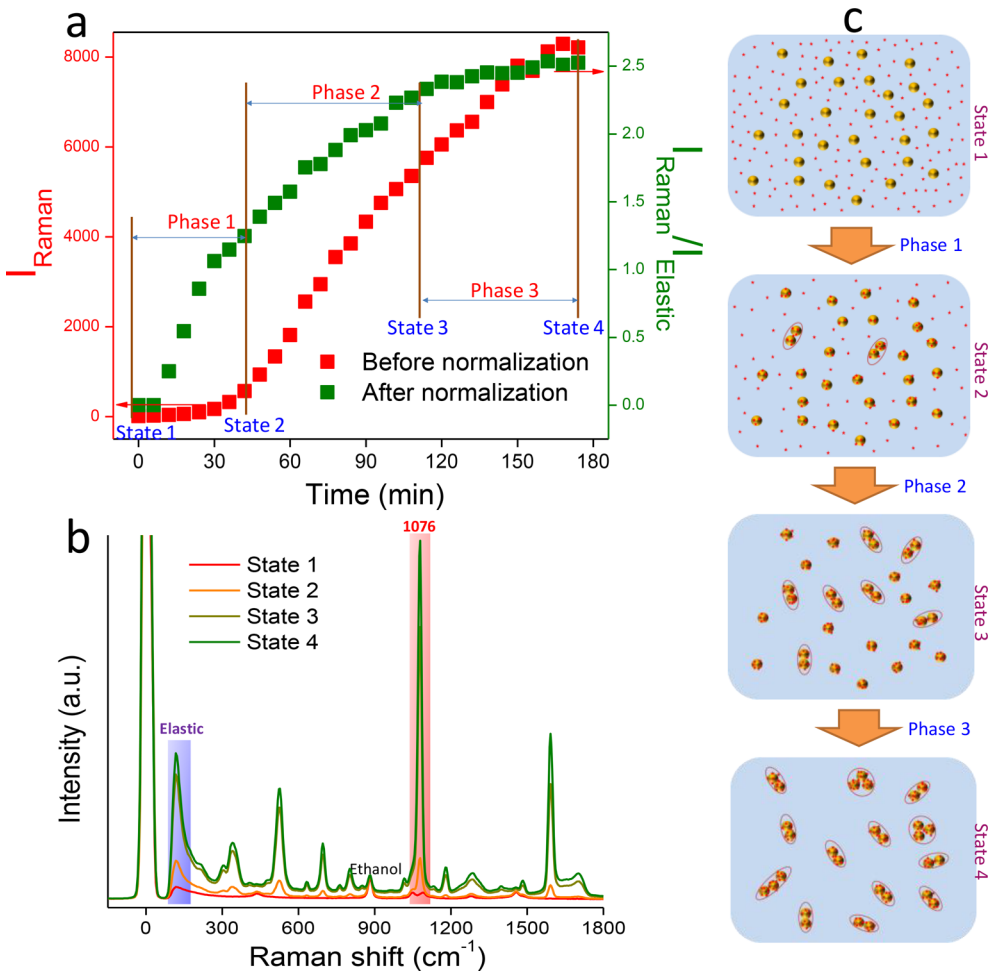

Figure 5. (a) Variation of SERS intensity of the Raman band at 1076 cm^{-1} of 4-MBA and the ratio of the Raman band at 1076 cm^{-1} to ν_e at 126 cm^{-1} (I_{1076}/I_{126}) as a function of time; (b) SERS spectra collected from the 4-MBA, AuNPs, and cosolvent system at the different stages marked in panel a; (c) Schematic of dynamic process of 4-MBA sorption to AuNP surface and AuNP aggregation.

alkanethiolate ligand-regulated AgNP film and using the ligand as internal standards.[17] The fact that HS normalization works well under challenging imaging conditions suggests even lower CV values can be achieved with nanoengineered substrates.

We have illustrated the applicability of HS normalization for analytes that strongly associate with the AuNP surface via a thiol linkage. However, many analytes only weakly associate with the surface via electrostatic interactions. Due to their lower surface affinities, these analytes present the greatest challenge for SERS based quantitation. To illustrate the broad applicability of HS normalization, SERS maps were acquired by scanning wet AuNP/BC substrates exposed to four structurally similar chloroanilines: 2-chloroaniline (2-CA), 3-chloroaniline (3-CA), 4-chloroaniline (4-CA), and 2,4-dichloroaniline (2,4-DCA). Across this series, the analyte pK_a value changes systematically due to inductive and deductive substituent effects.[53] A pH-triggered approach was applied to enhance surface affinity and ensure consistent molecular alignment on the AuNP surfaces (Figure S15).[7] Maps for 2-CA constructed by tracking the intensity of its characteristic band at 556 cm^{-1}, ν_e at 126 cm^{-1}, and the background PL at 1820 cm^{-1} are shown in Figure 3k–o. The CV of the SERS signals prior to HS normalization was 61.4%, but was reduced to 7.2% following normalization. Similar improvements in point-to-point variability were observed for the other chloroanilines (Figure S16).

ν_e-Enabled SERS Quantitation. The only factor that influences the ratio of the Raman and elastic scattering signals should be the molecular concentration of the target analyte within a "hot-spot". To illustrate, a piece of AuNP/BC hydrogel was fixed at the bottom of a Petri dish (Figure 4a). Immediately after adding 50 μM 4-MBA to the Petri dish, SERS spectra were collected over time. Prior to 4-MBA addition, only the ν_e signal was detected in the Raman spectrum (Figure 4b). Shortly following 4-MBA addition, the characteristic Raman bands of 4-MBA appear and increase with time. The HS normalized ratio (= I_{1076}/I_{84}) increases rapidly over the initial 30 min prior to plateauing after ~60 min (Figure 4c). The HS normalized reaction curves obtained using three batches of AuNP/BC virtually overlap, while substantial deviations were observed in the absence of HS normalization (Figure 4d). This result illustrates that HS normalization provides a reproducible means to monitor the adsorption kinetics of analytes onto a plasmonic nanoparticle surface. Such a result cannot be achieved by use of IEIS. Figure 4 suggests that HS normalization can be used to study the adsorption and desorption kinetics of many natural or synthetic compounds onto and from plasmonic surfaces.

To evaluate how analyte concentration alters the intensity of the SERS spectra, the concentrations of four chloroanilines

DOI: 10.1021/acs.analchem.7b04667
Anal. Chem. 2018, 90, 3227–3237

were varied over a range of 0.25−250 μM and their SERS spectra were collected (Figure S17). In the absence of HS normalization, the SERS intensities of the five prominent bands for 2,4-DCA generally increase with concentration (0.25−250 μM; Figure 4e), but exhibit substantial variability. Following HS normalization, the SERS intensities of these characteristic bands exhibit improved linear relationships versus their logarithmic concentrations (R^2 > 0.95) and substantially reduced error (Figure 4f). Similar results were achieved with three other chloroanilines (Supporting Information Figure S18) and a series of organic molecules (e.g., anilines with different functional groups, melamine, MGITC; Figure S19 and Note S3). These results show that HS normalization significantly improved the quantitation performance of SERS.

HS Normalization Enables Analyte Quantitation under Highly Variable Conditions. We have illustrated the capacity for HS normalization to quantify analyte adsorption to stable SERS substrates. To illustrate how HS normalization can be applied under dynamic conditions, we used it to quantify the kinetics of 4-MBA adsorption onto suspended AuNPs. The kinetics of AuNP aggregation in a water/ethanol cosolvent containing 4-MBA are easily controlled and were recently optimized for the production of SERS pH probes.[28] The lower dielectric constant of water/ethanol cosolvent, relative to water alone, facilitates 4-MBA mediated AuNP aggregation.[54] Following 4-MBA addition, the 4-MBA SERS signal increases only slightly during the first 40 min and then increases up to 162 min before plateauing (Figure 5a). It is well recognized that the increase in the number of 4-MBA molecules on the AuNP surface and the formation of "hot spots" due to AuNP aggregation simultaneously contribute to the enhancement in the SERS signal with time, but these two effects cannot be differentiated using existing approaches.

As shown by the green curve in Figure 5a, the HS normalized ratio (= I_{1076}/I_{126}) rapidly increases immediately after mixing of the AuNP suspension and 4-MBA solution (Phase 1). This increase continued until 114 min, albeit with a slower rate (Phase 2), prior to plateauing (Phase 3). To explain this process a schematic is shown in Figure 5c. At the very beginning, AuNPs were present as monomers with no 4-MBA on their surfaces (State 1). In State 1, the SERS spectrum only exhibits the Raman bands from ethanol (Figure 5b). State 2 is reached following 4-MBA adsorption in the first 40 min. In State 2, increasing numbers of 4-MBA molecules adsorb onto the AuNP surface, but most AuNPs remain as monomers. In this state, the Raman bands of 4-MBA appear, but are weak due to lack of "hot spots". In Phase 2, the surfaces become saturated with 4-MBA and large numbers of SERS "hot spots" form due to AuNP aggregation. This results in a very strong 4-MBA SERS signal for State 3. In Phase 3, fewer 4-MBA molecules remain available to associate with the AuNPs, yet "hot spots" continue to form. The increase in the 4-MBA SERS signal during Phase 3 is attributed primarily to "hot spot" formation and not continued 4-MBA adsorption.

CONCLUSIONS

Theoretical and experimental analysis suggests that ASE light elastically scattered by a SERS "hot spot" quantitatively reflects the integrated strength of the localized electromagnetic field. The ratio between the elastic and inelastic scattering signals is dependent on the number of the target analytes (N_A) within a "hot spot" regardless of how the size, shape, pattern, and density of plasmonic nanostructures varies. Surface-enhanced elastic scattering can be applied as a truly intrinsic internal standard for SERS. Following HS normalization, the uniformities of colloidal, hydrogel, and solid SERS substrates are improved without additional cost. Internal standards based on surface plasmon enhanced elastic scattering signals are truly intrinsic to the plasmonic nanostructures and provide new features that improve quantitative SERS analysis: (1) ultimate photostability (i.e., not photobleachable); (2) minimal spectral interference by analyte Raman signals; (3) no spatial competition with analyte molecules for SERS "hot spots"; (4) reduced SERS substrate preparation costs by avoiding the incorporation of extrinsic reference probe molecules molecules; (5) universal applicability for a suite of SERS substrates; and (6) the capacity to differentiate analyte adsorption and "hot spot" formation under dynamic conditions. We close by noting that while HS normalization can provide improved quantitation that it nonetheless remains highly important that the affinity of any given analyte to the plasmonic surface as well as the impacts of potential interferents are fully considered when determining concentration.

ASSOCIATED CONTENT

Supporting Information

The Supporting Information is available free of charge on the ACS Publications website at DOI: 10.1021/acs.analchem.7b04667.

SEM, EDS, and UV−vis spectra of the SERS substrates; additional SERS spectra of different substrate, different edge filters, baseline correction, and different analytes; SERS spectra of anilines with different concentrations and 50 randomly selected spectra from their SERS maps; additional maps before and after "hot spot" normalization for suspension-based substrates, hydrogel substrates in different areas, and different analytes; tables show the Raman band assignment and CV values reported in literature; and notes describe the experimental details (PDF)

AUTHOR INFORMATION

Corresponding Author

*Phone: (540) 231-3568, E-mail: pvikes@vt.edu.

ORCID

Linsey C. Marr: 0000-0003-3628-6891

Peter J. Vikesland: 0000-0003-2654-5132

Notes

The authors declare no competing financial interest.

ACKNOWLEDGMENTS

This research was supported by the National Institutes of Health (NIH) through the NIH Director's New Innovator Award Program (1-DP2-A1112243) to L.M. and through US National Science Foundation grants CBET-1133746 and OISE-1545756 to P.V. Additional support for H.W. and M.W. was provided by the Virginia Tech Graduate School through the Sustainable Nanotechnology Interdisciplinary Graduate Education Program (VT-SuN IGEP). W.Z. and J.S. are supported by startup funds from Virginia Tech. We thank K. Rodriguez and S. Renneckar for their help with production of BC.

REFERENCES

(1) Schlücker, S. *Angew. Chem., Int. Ed.* **2014**, *53*, 4756−4795.

DOI: 10.1021/acs.analchem.7b04667
Anal. Chem. 2018, 90, 3227−3237

(2) De Angelis, F.; Gentile, F.; Mecarini, F.; Das, G.; Moretti, M.; Candeloro, P.; Coluccio, M.; Cojoc, G.; Accardo, A.; Liberale, C.; et al. *Nat. Photonics* **2011**, *5*, 682−687.
(3) Kneipp, K.; Wang, Y.; Kneipp, H.; Perelman, L. T.; Itzkan, I.; Dasari, R. R.; Feld, M. S. *Phys. Rev. Lett.* **1997**, *78*, 1667.
(4) Nie, S.; Emory, S. R. *Science* **1997**, *275*, 1102−1106.
(5) Sharma, B.; Frontiera, R. R.; Henry, A.-I.; Ringe, E.; Van Duyne, R. P. *Mater. Today* **2012**, *15*, 16−25.
(6) Liu, H.; Yang, Z.; Meng, L.; Sun, Y.; Wang, J.; Yang, L.; Liu, J.; Tian, Z. *J. Am. Chem. Soc.* **2014**, *136*, 5332−5341.
(7) Wei, H.; Vikesland, P. J. *Sci. Rep.* **2016**, *5*, 18131.
(8) Alabi, O.; Edilbi, A.; Brolly, C.; Muirhead, D.; Parnell, J.; Stacey, R.; Bowden, S. *Chem. Commun.* **2015**, *51*, 7152−7155.
(9) Wei, H.; Abtahi, S. M. H.; Vikesland, P. J. *Environ. Sci.: Nano* **2015**, *2*, 120−135.
(10) Abu Hatab, N. A.; Oran, J. M.; Sepaniak, M. J. *ACS Nano* **2008**, *2*, 377−385.
(11) Li, J. F.; Huang, Y. F.; Ding, Y.; Yang, Z. L.; Li, S. B.; Zhou, X. S.; Fan, F. R.; Zhang, W.; Zhou, Z. Y.; Wu, D. Y.; et al. *Nature* **2010**, *464*, 392−395.
(12) Lim, D. K.; Jeon, K. S.; Hwang, J. H.; Kim, H.; Kwon, S.; Suh, Y. D.; Nam, J. M. *Nat. Nanotechnol.* **2011**, *6*, 452−460.
(13) Jin, Y. *Adv. Mater.* **2012**, *24*, 5153−5165.
(14) Qin, L.; Zou, S.; Xue, C.; Atkinson, A.; Schatz, G. C.; Mirkin, C. A. *Proc. Natl. Acad. Sci. U. S. A.* **2006**, *103*, 13300−13303.
(15) Alvarez-Puebla, R. A.; Agarwal, A.; Manna, P.; Khanal, B. P.; Aldeanueva-Potel, P.; Carbó-Argibay, E.; Pazos-Pérez, N.; Vigderman, L.; Zubarev, E. R.; Kotov, N. A.; Liz-Marzan, L. M. *Proc. Natl. Acad. Sci. U. S. A.* **2011**, *108*, 8157−8161.
(16) Guttler, B.; Zakel, S.; Wundrack, S.; Stosch, R. *Handbook of Enhanced Spectroscopy*; Pan Stanford: Singapore, 2015; pp 307−328.
(17) Chen, H. Y.; Lin, M. H.; Wang, C. Y.; Chang, Y. M.; Gwo, S. *J. Am. Chem. Soc.* **2015**, *137*, 13698−13705.
(18) Shen, W.; Lin, X.; Jiang, C.; Li, C.; Lin, H.; Huang, J.; Wang, S.; Liu, G.; Yan, X.; Zhong, Q.; Ren, B. *Angew. Chem.* **2015**, *127*, 7416−7420.
(19) Zhang, D.; Xie, Y.; Deb, S. K.; Davison, V. J.; Ben-Amotz, D. *Anal. Chem.* **2005**, *77*, 3563−3569.
(20) Itoh, N.; Bell, S. E. *Analyst* **2017**, *142*, 994−998.
(21) Bell, S. E.; Sirimuthu, N. M. *Chem. Soc. Rev.* **2008**, *37*, 1012−1024.
(22) Blackie, E. J.; Ru, E. C. L.; Etchegoin, P. G. *J. Am. Chem. Soc.* **2009**, *131*, 14466−14472.
(23) Jarvis, R. M.; Goodacre, R. *Anal. Chem.* **2004**, *76*, 40−47.
(24) Qian, X.; Peng, X.-H.; Ansari, D. O.; Yin-Goen, Q.; Chen, G. Z.; Shin, D. M.; Yang, L.; Young, A. N.; Wang, M. D.; Nie, S. *Nat. Biotechnol.* **2008**, *26*, 83.
(25) Zavaleta, C. L.; Smith, B. R.; Walton, I.; Doering, W.; Davis, G.; Shojaei, B.; Natan, M. J.; Gambhir, S. S. *Proc. Natl. Acad. Sci. U. S. A.* **2009**, *106*, 13511−13516.
(26) Camden, J. P.; Dieringer, J. A.; Zhao, J.; Van Duyne, R. P. *Acc. Chem. Res.* **2008**, *41*, 1653−1661.
(27) Alonso-González, P.; Albella, P.; Schnell, M.; Chen, J.; Huth, F.; García-Etxarri, A.; Casanova, F.; Golmar, F.; Arzubiaga, L.; Hueso, L.; et al. *Nat. Commun.* **2012**, *3*, 684.
(28) Wei, H.; Willner, M. R.; Marr, L. C.; Vikesland, P. J. *Analyst* **2016**, *141*, 5159−5169.
(29) Novotny, L.; Hecht, B. *Principles of Nano-Optics*; Cambridge University Press: Cambridge, U.K., 2012.
(30) Efrima, S.; Metiu, H. *J. Chem. Phys.* **1979**, *70*, 1602−1613.
(31) Wall, K. F.; Chang, R. K. *Opt. Lett.* **1986**, *11*, 493−495.
(32) Lumdee, C.; Yun, B.; Kik, P. G. *ACS Photonics* **2014**, *1*, 1224−1230.
(33) Maruyama, Y.; Futamata, M. *J. Raman Spectrosc.* **2005**, *36*, 581−592.
(34) Lin, K.-Q.; Yi, J.; Zhong, J.-H.; Hu, S.; Liu, B.-J.; Liu, J.-Y.; Zong, C.; Lei, Z.-C.; Wang, X.; Aizpurua, J.; et al. *Nat. Commun.* **2017**, *8*, 14891.
(35) Galloway, C.; Etchegoin, P.; Le Ru, E. *Phys. Rev. Lett.* **2009**, *103*, 063003.
(36) Hu, H.; Duan, H.; Yang, J. K.; Shen, Z. X. *ACS Nano* **2012**, *6*, 10147−10155.
(37) Buchanan, S.; Le Ru, E.; Etchegoin, P. *Phys. Chem. Chem. Phys.* **2009**, *11*, 7406−7411.
(38) Le Ru, E.; Etchegoin, P.; Grand, J.; Felidj, N.; Aubard, J.; Levi, G. *J. Phys. Chem. C* **2007**, *111*, 16076−16079.
(39) Shahbazyan, T. V. *Nano Lett.* **2013**, *13*, 194−198.
(40) Mahajan, S.; Cole, R. M.; Speed, J. D.; Pelfrey, S. H.; Russell, A. E.; Bartlett, P. N.; Barnett, S. M.; Baumberg, J. J. *J. Phys. Chem. C* **2010**, *114*, 7242−7250.
(41) Jiang, J.; Bosnick, K.; Maillard, M.; Brus, L. *J. Phys. Chem. B* **2003**, *107*, 9964−9972.
(42) Eilers, P. H. *Anal. Chem.* **2004**, *76*, 404−411.
(43) Guan, Z.; Gao, N.; Jiang, X.-F.; Yuan, P.; Han, F.; Xu, Q.-H. *J. Am. Chem. Soc.* **2013**, *135*, 7272−7277.
(44) Bouhelier, A.; Bachelot, R.; Lerondel, G.; Kostcheev, S.; Royer, P.; Wiederrecht, G. *Phys. Rev. Lett.* **2005**, *95*, 267405.
(45) Campion, A.; Kambhampati, P. *Chem. Soc. Rev.* **1998**, *27*, 241−250.
(46) Yamamoto, Y. S.; Hasegawa, K.; Hasegawa, Y.; Takahashi, N.; Kitahama, Y.; Fukuoka, S.; Murase, N.; Baba, Y.; Ozaki, Y.; Itoh, T. *Phys. Chem. Chem. Phys.* **2013**, *15*, 14611−14615.
(47) Boyd, G.; Yu, Z.; Shen, Y. *Phys. Rev. B: Condens. Matter Mater. Phys.* **1986**, *33*, 7923.
(48) Michaels, A. M.; Nirmal, M.; Brus, L. *J. Am. Chem. Soc.* **1999**, *121*, 9932−9939.
(49) Yoshida, K.-i.; Itoh, T.; Tamaru, H.; Biju, V.; Ishikawa, M.; Ozaki, Y. *Phys. Rev. B: Condens. Matter Mater. Phys.* **2010**, *81*, 115406.
(50) Huang, J. A.; Zhao, Y. Q.; Zhang, X. J.; He, L. F.; Wong, T. L.; Chui, Y. S.; Zhang, W. J.; Lee, S. T. *Nano Lett.* **2013**, *13*, 5039−5045.
(51) Lin, D.; Wu, Z.; Li, S.; Zhao, W.; Ma, C.; Wang, J.; Jiang, Z.; Zhong, Z.; Zheng, Y.; Yang, X. *ACS Nano* **2017**, *11*, 1478−1487.
(52) Yan, B.; Thubagere, A.; Premasiri, W. R.; Ziegler, L. D.; Dal Negro, L.; Reinhard, B. M. *ACS Nano* **2009**, *3*, 1190−1202.
(53) Schwarzenbach, R. P.; Gschwend, P. M.; Imboden, D. M. *Environmental Organic Chemistry*; John Wiley & Sons, Inc.: Hoboken, NJ, 2005.
(54) Zhang, Y.; Li, X.; Xue, B.; Kong, X.; Liu, X.; Tu, L.; Chang, Y. *Sci. Rep.* **2015**, *5*, 14934.

DOI: 10.1021/acs.analchem.7b04667
Anal. Chem. 2018, 90, 3227−3237